Quench Detection in Insulated, NI, and MI $(RE)Ba_2Cu_3O_{7-x}$ Coils with Superconducting Quench Detectors

Shin Hasegawa, *Member*, *IEEE*, Satoshi Ito, Gen Nishijima, Satoshi Awaji, Kohki Takahashi and Hidetoshi Hashizume

***Abstract*— We have proposed a quench detection method that uses a low-temperature superconducting quench detector (LTS QD) for rare-earth barium copper oxide (REBCO) coils at 4.2 K. Previous studies demonstrated the quench detection with a LTS QD in a layer-wound REBCO coil. In this study, the quench detection performance of LTS QDs for insulated, no-insulation (NI), and metal-as-insulation (MI) REBCO pancake coils was experimentally compared. An experiment that used a Nb–Ti/Cu–Ni QD installed in insulated, NI, and MI REBCO coils demonstrated a quench detection before a thermal runaway in the coil at 4.2 K and 0–9 T. Nb–Ti/Cu–Ni QD showed slower quench detection in the coils without turn-to-turn insulation. It would be due to the small heat density around the hot spot and large heat exchange between the Nb–Ti/Cu–Ni QD and REBCO coils. In conclusion, this study indicated that the turn-to-turn resistance in the REBCO coil and thermal gap conductance between the coil and LTS QD are key parameters for the design of LTS QDs. Moreover, feasibility of the quench detection with appropriate LTS QDs for the insulated, NI, and MI REBCO pancake coils was demonstrated at 4.2 K.**

Index Terms— quench detection, quench protection, REBCO coil, no-insulation coil, metal-as-insulation coil, superconducting quench detector, Nb–Ti[1]

I. Introduction

Quench detection is important for a high-temperature superconducting (HTS) coil—for example, a rare-earth barium copper oxide (REBCO) coil—cooled with 4.2 K liquid helium (LHe) for high magnetic field application. A conventional quench detection method for superconducting coils is a direct voltage measurement. However, the normal zone propagation velocity in the HTS coil is 100–1000 times slower than that of low-temperature superconducting (LTS) coil [1]–[4]. Thus, detectable voltage in the HTS coil would be smaller than the quench detection criterion (> 0.1 V [5], [6]), which may lead to burning out of the coil. To address this issue, various new quench detection methods [7]–[27] have been proposed, as presented in Table I. Here, "insulated pancake coil" means the pancake coil with turn-to-turn insulation. However, only few cases were reported on the experimental demonstration at 4.2 K. Moreover, quench detection for the HTS coil without turn-to-turn electrical insulation—that is, no-insulation (NI) [28]–[33] and metal-as-insulation (MI) [34]–[36] coils—was reported in a small number of literature. These coils are considered more thermally stable than insulated coils. However, the actual protection performance of the NI and MI techniques is under investigation, and quench detection and active protection for these coils remains important in terms of failing safety [37].

Table I Proposed quench detection method for HTS coil

Method	Operation temperature for experimental demonstration		
	Tape / cable / solenoid	Insulated pancake coil	NI/MI pancake coils
Secondary magnetic coupled coils	-	77 K [7]–[9]	20 K [10]
Poynting vectors	-	77 K [11], [12]	-
Acoustic signals (active and passive)	77 K [13]–[15]	77 K [16], [17]	-
Optical fiber sensors	14–77 K [18]–[23]	-	77 K [24] –[26]
Turn-to-turn capacitance	-	4.2 K [27]	-

Our previous works [38]–[40] proposed using superconducting quench detectors (QDs) [41], [42], which were LTS composite wires (LTS QDs), for REBCO coils operated at 4.2 K. Bias currents (monitoring current, I_m) flow in the electrically insulated LTS QDs. Heat from a hot spot in the REBCO coil would lead the current sharing and voltage rises in the LTS QDs. If the voltage becomes sufficiently larger than the threshold voltage, detecting the quench before the thermal runaway in the REBCO coil is possible. Quench detection before thermal runaway in a REBCO tape and an insulated REBCO coil ("quick quench detection") has been demonstrated by using Nb–Ti QDs at 4.2 K and 0–9 T [38]–[40]. Recently, it has also been suggested to apply the superconducting quench detector with similar concept for the HTS applications [43]–[46].

This work was supported by the Grant-in-Aid for Japan Society for the Promotion of Science (JSPS) Fellows under Grant 19J10989 and JSPS Grant-in-Aid for Scientific Research (B) under Grant JP17H03507 and 20H01884 (Corresponding author: Shin Hasegawa).

S. Hasegawa is with National Institutes for Quantum Science and Technology, Naka 311-0193, Japan, and ITER Organization, St. Paul Lez Durance 13067, France (e-mail: hasegawa.shin2@qst.go.jp)

S. Ito and H. Hashizume are with Department of Quantum Science and Energy Engineering, Graduate School of Engineering, Tohoku University, Sendai 980-8577, Japan (e-mail: satoshi.ito.e3@tohoku.ac.jp; hidetoshi.hashizume.a5@tohoku.ac.jp).

G. Nishijima is with National Institute for Materials Science, Tsukuba 305-0003, Japan (e-mail: NISHIJIMA.Gen@nims.go.jp)

S. Awaji and K. Takahashi are with High Field Laboratory for Superconducting Materials, Institute for Materials Research, Tohoku University, Sendai 980-8577, Japan (e-mail: awaji@tohoku.ac.jp; kohki.takahashi.e5@tohoku.ac.jp).

However, the quench detectability of the LTS QDs for the REBCO pancake coil under magnetic field has not been experimentally investigated. A past experiment [39] demonstrated a quench detection with the Nb–Ti QD with ~2 seconds margin before the thermal runaway in the insulated REBCO coil. Considering the risk of delay in the protection system, more time margin would be desired for safer quench protection by damping the coil current with a few seconds to minutes. In a practical operation environment, a magnetic field will increase the load factor of the LTS QD resulting in its quicker response with more margin as anticipated in [40]. A further interest is the performance of LTS QD in the NI and MI REBCO coils. Compared with the insulated coil, heat density around the hot spot becomes less in the NI and MI coils, which may lead to a delay in the response of the LTS QD. Although this study focuses on only the Nb-Ti QD, key parameters of the behavior of LTS QDs made of other superconductors, such as Nb_3Al, MgB_2, and iron-based superconductors, would be similar. Comprehension of the behavior of the LTS QD in the REBCO coils with different physical characteristics is crucial to formulate an universal design strategy for the LTS QD.

We experimentally compared the quench detection performance of Nb–Ti/Cu–Ni QD for insulated, NI, and MI REBCO pancake coils cooled in 4.2 K LHe bath at 0–9 T. Section II describes the experimental method. Section III presents the results and discussion, followed by a conclusion in Section IV.

II. Experiment

A. Sample fabrications

Three types of 20-turn REBCO single pancake coils (i.e., insulated, NI, and MI) were fabricated to demonstrate quick quench detection with LTS QDs. Previous studies indicated that LTS QDs with a high normal resistance are suitable for this method [38], [40]. Thus, a formal-insulated Nb–Ti wire with a Cu–Ni matrix (Supercon, SW-18) was chosen as the LTS QD (Nb–Ti/Cu–Ni QD). Fig. 1 shows a schematic view of the REBCO coil samples, in which a 4-mm-wide REBCO tape (SuperPower, SC4050) was wound on a glass fiber reinforced plastic (GFRP) bobbin. Fig. 2 shows the fabricated insulated, NI, and MI coils. For the insulated REBCO coil, a polyimide tape and the Nb–Ti/Cu–Ni QD were co-wound with the

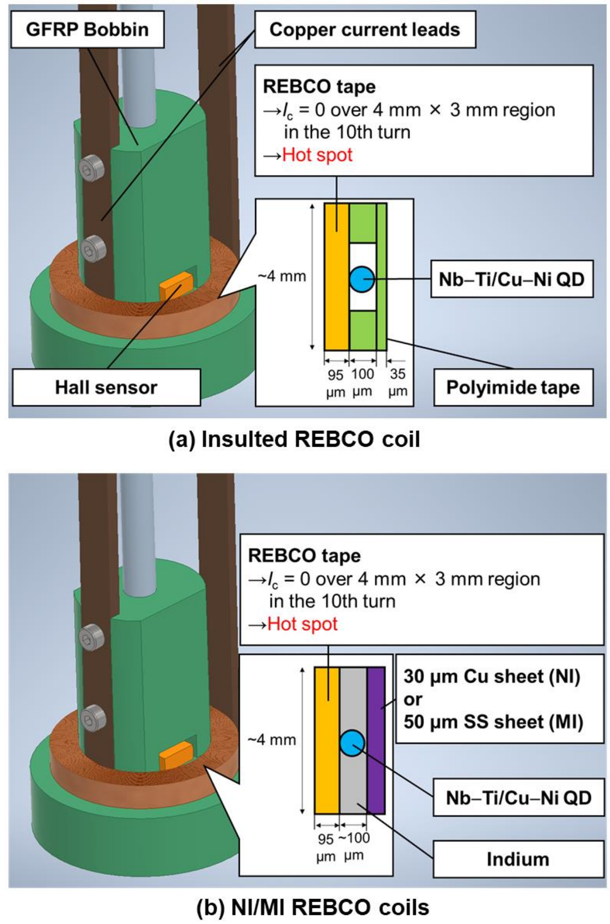

Fig. 1 Schematic views of the REBCO coil samples; (a) insulated REBCO coil and (b) NI/MI REBCO coils

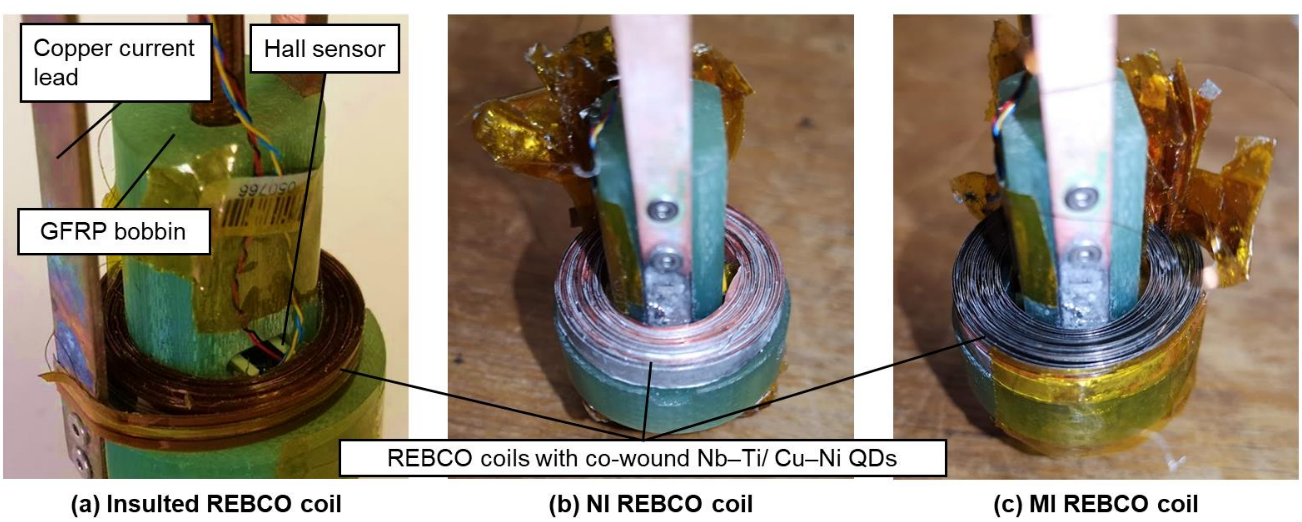

Fig. 2 Fabricated REBCO coil samples; (a) insulated, (b) NI, and (c) MI REBCO coils

Table II Specifications of the three types of REBCO coils samples: insulated, NI, and MI coils.

Items	Values		
	Insulated	NI	MI
Conductor width / thickness	4.0 mm / 95 μm	4.0 mm / 95 μm	4.0 mm / 95 μm
I_c at 77 K, s.f.	~126 A	~126 A	~126 A
Thickness of indium sheet	-	100 μm	100 μm
Thickness of turn-to-turn insert	135 μm (Polyimide)	30 μm (Cu)	50 μm (Stainless steel)
Width of turn-to-turn insert	4 mm	4 mm	6 mm
Inner diameter	20 mm	20 mm	20 mm
Outer diameter	24.7 mm	28.5 mm	29.1 mm
Total turns	20	20	20
Coil inductance	~13 μH	~13 μH	~13 μH

Table III Specification of the Nb–Ti/Cu–Ni QD

Items	Values
Diameter (bare / insulated)	75 μm / 100 μm
Stabilizer	$Cu_{0.9}$–$Ni_{0.1}$
Stabilizer ratio	1.5
Filament diameter	11 μm
Filament number	18
I_c at 4.2 K, 9 T	~0.81 A

REBCO tape. In the past experiment [39], the Nb–Ti/Cu–Ni QD was attached only on the outmost surface of the pancake coil. This arrangement could possibly lead to the delay in quench detection due to the long distance from the hot spot to the Nb–Ti/Cu–Ni QD. The co-winding method enables the LTS QD to be positioned in proximity to any hot spot location, allowing quicker quench detection. For the NI and MI coils, a 100-μm-thick indium foil, the Nb–Ti/Cu–Ni QD, and a metal insert (Cu or 301 stainless steel (SS)) were co-wound with the REBCO tape. The Nb–Ti/Cu–Ni QD embedded in the indium foil is similar to an optical fiber installed in a REBCO tape [19]. The configuration of the NI coil in this experiment corresponds to the one with co-wound materials as shown in [47], [48]. A 4-mm-wide and 30-μm-thick Cu sheet, and 6-mm-wide and 50-μm-thick SS sheet were used for the NI and MI coils, respectively, as metal inserts between coil turns. Side of the MI coil was not smooth since the width of SS sheet was 2 mm larger than that of REBCO tape as shown in Fig. 2 (c). In real case, the MI coil can be stacked by using the REBCO tapes and SS tapes with the same width. Note that, a sufficiently thin LTS QD shall be installed in the turn-to-turn materials to prevent a decrease in engineering current density of the REBCO coil also in the practical applications. Alternatively, placing the LTS QD on the side surface of the REBCO coil is also a viable option [44].

Table II and Table III list the specifications of the REBCO coils and Nb–Ti/Cu–Ni QDs, respectively. Local defects due to the insufficient homogeneity in the tape can lead to the unexpected quench of the REBCO coil [37]. In this study, therefore, we made a local degradation in the REBCO coil assuming the unexpected quench during the magnet excitation. The critical current (I_c) of a 4-mm-wide × 3-mm-long region in the 10th turn was degraded to 0 A with a compressive force of 2000 N. The distance between the voltage taps was 1470 mm for both the REBCO coil (V_{RE}) and Nb–Ti QD (V_{QD}).

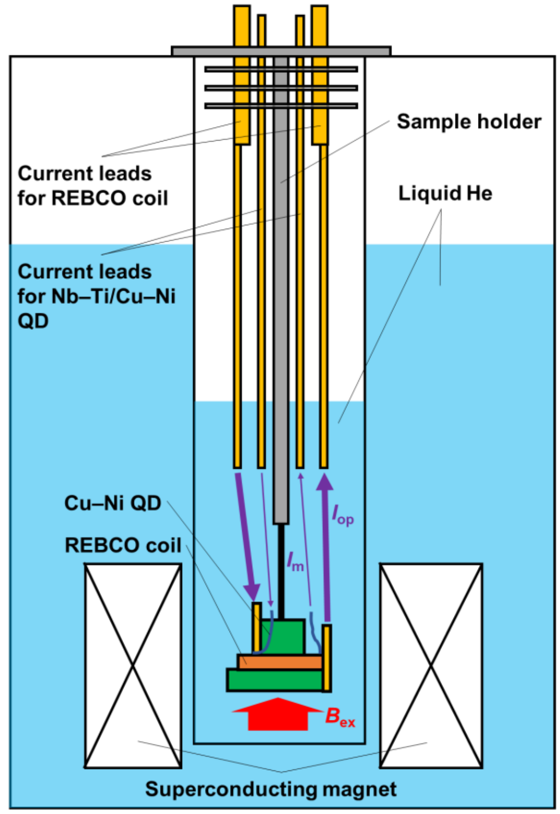

Fig. 3 Experimental setup where the sample was immersed in LHe and magnetic field was applied to the sample by an external superconducting magnet

Table IV Operation conditions of the Nb–Ti/Cu–Ni QD where the load factor of I_m depends on B_{ex}

I_m	B_{ex}	Load factor of I_m	T_{cs}
	0 T	0.01	9.4 K
0.31 A	5 T	0.062	9.2 K
	9 T	0.38	7.5 K

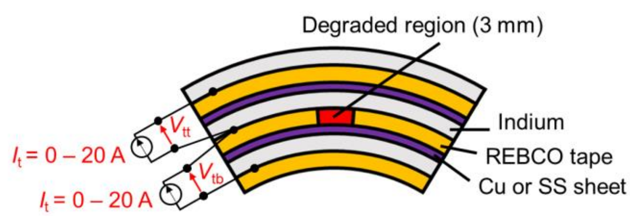

Fig. 4 Measurement of turn-to-turn resistance in the NI/MI REBCO coils where the turn-to-turn voltages (V_{tt} and V_{tb}) were measured by applying the current (I_t)

B. Experimental setup

Fig. 3 shows the experimental setup. The REBCO coil sample was set on the sample holder, which was immersed in an LHe bath in an inner dewar of the 15-T superconducting magnet. Nb–Ti/Cu–Ni QD would be used at less than 10 T considering its critical current. Thus, the magnetic field around the REBCO coil (B_{ex}) was set to 0, 5, and 9 T in this experiment. I_m for the Nb–Ti/Cu–Ni QD was determined by using the procedure described in [40]. Table IV shows I_m, B_{ex} dependence of its load factor (= I_m/I_c), and current sharing temperature (T_{cs}). Operation current in the REBCO coil (I_{op}) was ramped up from 0 A with a certain sweep rate (α_{op}). The current sources for REBCO coil and LTS QD were manually shut down after the quench detection. Exceptionally, an interlock system of the current source interrupted the current at the detection of open circuit. I_m of the LTS QD should be dumped after the quench detection to avoid its burning out also in the practical application.

I_{op} at quench detection (I_{opQD}) would depend on α_{op} with the following reason. We now consider a lumped-capacitance model of the hot spot in the REBCO coil where influence of three-dimensional thermal diffusion is not taken into account. Then, the following heat-balance equation holds,

$$C_{tape}\frac{\mathrm{d}T_{hs}}{\mathrm{d}t} = \rho_{tape}\left(\frac{I_{op}}{A_{tape}}\right)^2 = \frac{\rho_{tape}}{A_{tape}^2}\alpha_{op}^2 t^2, \qquad (1)$$

where T_{hs}, C_{tape}, ρ_{tape}, t, and A_{tape} are hot-spot temperature, heat capacity and resistivity of the REBCO tape at normal state, time, and the cross-sectional area of the REBCO tape, respectively. Integrating the equation (1) from $t = 0$ ($T_{hs} = T_{op}$) to $t = t_{QD}$ ($T_{hs} = T_{hsQD}$), it yields

$$T_{hsQD} = \frac{\rho_{tape}\alpha_{op}^2 t_{QD}^3}{3A_{tape}^2 C_{tape}} + T_{op} = \frac{\rho_{tape}}{3A_{tape}^2 C_{tape}}\frac{I_{opQD}^3}{\alpha_{op}} + T_{op}, \qquad (2)$$

where t_{QD}, T_{op} and T_{opQD} are t at quench detection, operation temperature, and T_{hs} at $t = t_{QD}$. When ρ_{tape}, C_{tape}, A_{tape}, and T_{hsQD} are the constants, I_{opQD} should be proportional to 1/3 power of α_{op}. For this reason, α_{op} would be the influential parameter on the quench detection performance of LTS QD. Thus, α_{op} was set to 1, 5, and 10 A/s for the insulated REBCO coil to determine its influence on the LTS-QD performance; it was fixed at 10 A/s for NI/MI coils.

The current distribution in the NI and MI REBCO coils evaluated with turn-to-turn resistance is important to know which heat leads to the quench in the LTS QD. Fig. 4 shows that, in the NI and MI REBCO coils, additional taps (V_{tt} and V_{tb}) were installed at two locations around the degraded region to measure the turn-to-turn resistance before the quench detection experiment. 30-µm-thick copper sheets used for V_{tt} and V_{tb} were soldered to the REBCO tape or indium foil. The bonding surface of the voltage taps was 1 mm × 3 mm.

PSW-720H800 (TEXIO TECHNOLOGY CORP., Yokohama, Japan) and PAS16-500LS (KIKUSUI ELEC TRONICS CORP., Yokohama, Japan) constant current sources supplied the current to the Nb–Ti/Cu–Ni QD and the REBCO coil, respectively. The sample voltages were recorded by using an MR8741 data logger (HIOKI E.E. CORP., Ueda, Japan) with a sampling rate of 200 Hz. The background noise was in the order of 10^{-5}–10^{-3} V in our experimental environment. 0.1 V was used as a quench detection criterion [5], [6].

III. Results and Discussion

A. Quench detection performance of Nb-Ti/Cu-Ni QD for insulated REBCO coil

Time margin from the conventional quench detection to the thermal runaway in the insulated REBCO coil was first confirmed prior to the experiment with the LTS QD. Fig. 5 shows the voltage V_{RE} and operation current I_{op} in the REBCO coil when thermal runaway occurred in the REBCO coil with α_{op} = 10 A/s at B_{ex} = 9 T. V_{RE} started to rapidly increase at I_{op} ~172 A (19.4 s), and the coil was finally burned out in the degraded region. This localized thermal runaway is reasonable because I_c of the REBCO tape except in the degraded area is ~400 A at 4.2 K and 9 T considering its temperature and field dependence [49][50]. The coil current was automatically damped since the open circuit of the burned coil was detected by the current source. V_{RE} exceeds 0.1 V also at I_{op} ~172 A (20 s). The time margin for the quench protection is less than 1 second due to the rapid thermal runaway in the coil, and the conventional method may lead to the failure of coil protection considering the delay of protection system.

A quench detection experiment was performed with a new insulated coil where the Nb–Ti/Cu–Ni QD was co-wound. Table V lists the t_{QD} and I_{opQD} at 0.1 V detection by the LTS QDs for different B_{ex} and α_{op} in all the REBCO coils. The

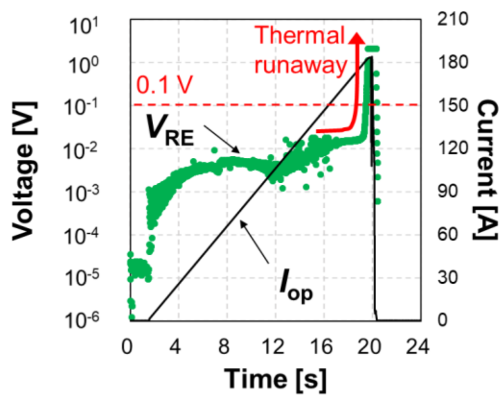

Fig. 5 Quench detection with the conventional method and thermal runaway in the insulated REBCO coil at α_{op} = 10 A/s and B_{ex} = 9 T

Table V t_{QD} and I_{opQD} at 0.1 V detection by LTS QD for different external magnetic fields (B_{ex}) and current ramping rates (α_{op}) in the insulated, NI, and MI REBCO coils

Coils	B_{ex}	α_{op}	t_{QD}	I_{opQD}
Insulated	0 T	10 A/s	9.6 s	92.3 A
		5 A/s	18.6 s	91.9 A
		1 A/s	102 s	91.7 A
	5 T	10 A/s	6.5 s	61.9 A
		5 A/s	12.8 s	62.6 A
		1 A/s	69.5 s	61.4 A
	9 T	10 A/s	4.8 s	47.0 A
		5 A/s	9.2 s	44.2 A
		1 A/s	51.8 s	43.9 A
NI	0 T	10 A/s	45.8 s	472 A
	5 T	10 A/s	30.8 s	313 A
	9 T	10 A/s	16.9 s	133 A
MI	0 T	10 A/s	14.4 s	147 A
	5 T	10 A/s	12.4 s	109 A
	9 T	10 A/s	8.4 s	79.7 A

results for the NI and MI REBCO coils are discussed in the next sub-section. I_{opQD} decreased with the increasing field due to the load factor of I_m and T_{cs} as shown in Table IV. Fig. 6 shows V_{RE}, V_{QD}, and I_{op} at 0 T, 5 T, and 9 T when α_{op} = 10 A/s. V_{QD} exceeds 0.1 V when I_{op} (time) was 92.3 A (9.6 s), 61.9 A (6.5 s), and 47.0 A (4.8 s) at 0 T, 5 T, and 9 T, respectively. Nb–Ti/Cu–Ni QD quickly detected quench in the insulated REBCO coil at B_{ex} = 0–9 T, as well as in the case of the REBCO tape [41]. Assuming the result of thermal runaway in the REBCO coil shown in Fig. 5, the Nb–Ti/Cu–Ni QD (Fig. 6 (c)) was able to detect the quench with a 13.5-seconds margin before the thermal runaway at B_{ex} = 9 T and α_{op} = 10 A/s.

We also compared the quench detection sensitivity of the Nb–Ti/Cu–Ni QD with respect to the α_{op}. Fig. 7 and Fig. 8 show V_{RE}, V_{QD}, and I_{op} at 0–9 T when α_{op} = 5 A/s and 1 A/s, respectively. In the case α_{op} = 5 A/s, 0.1 V was detected when I_{op} (time) was 91.9 A (18.6 s), 62.6 A (12.8 s), and 44.2 A (9.2 s) at 0 T, 5 T, and 9 T, respectively. In the case α_{op} = 1 A/s, 0.1 V was detected when I_{op} (time) was 91.7 A (102 s), 61.4 A (69.5 s), and 43.9 A (51.8 s) at 0 T, 5 T, and 9 T, respectively. I_{opQD} varied only by 1.2%–6.2% difference in the range of α_{op} = 1 A/s–10 A/s. Thus, the quench detection performance of the LTS QD does not depend on the operating conditions of the REBCO coil. This would be because three-dimensional heat diffusion from the hot spot led to the gradual increase of the hot-spot temperature in the REBCO coil, which is not considered in the equations (1) and (2) of the lumped-capacitance model. It then resulted in weak α_{op} dependence of I_{opQD}.

Moreover, the result at α_{op} = 1 A/s suggests the Nb–Ti/Cu–Ni QD detects the quench more than one minute before the

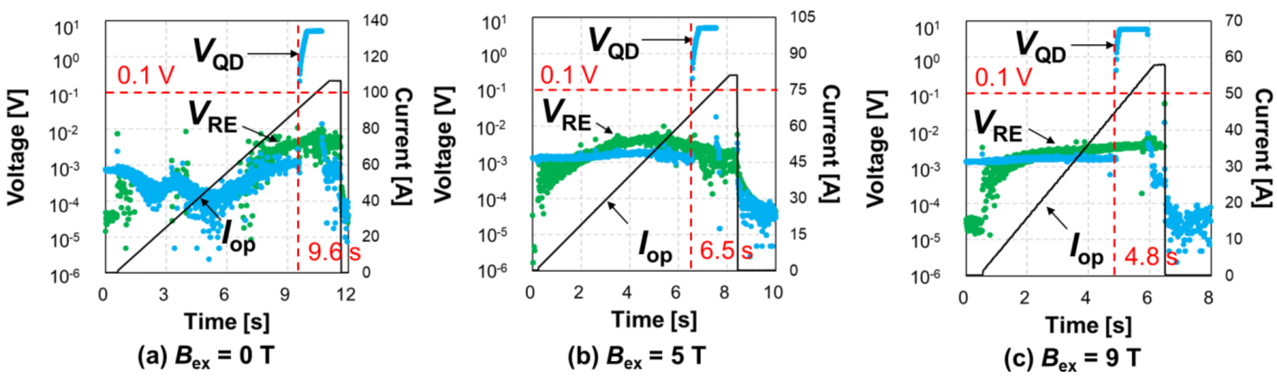

Fig. 6 Results of quench detection experiment with insulated REBCO coil at α_{op} = 10 A/s: (a) B_{ex} = 0 T, (b) B_{ex} = 5 T, and (c) B_{ex} = 9 T

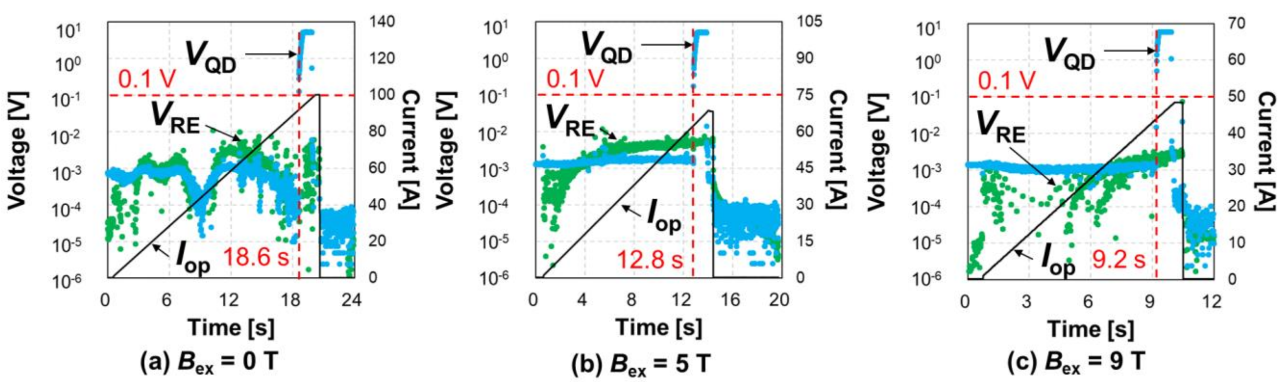

Fig. 7 Results of quench detection experiment with insulated REBCO coil at α_{op} = 5 A/s: (a) B_{ex} = 0 T, (b) B_{ex} = 5 T, and (c) B_{ex} = 9 T

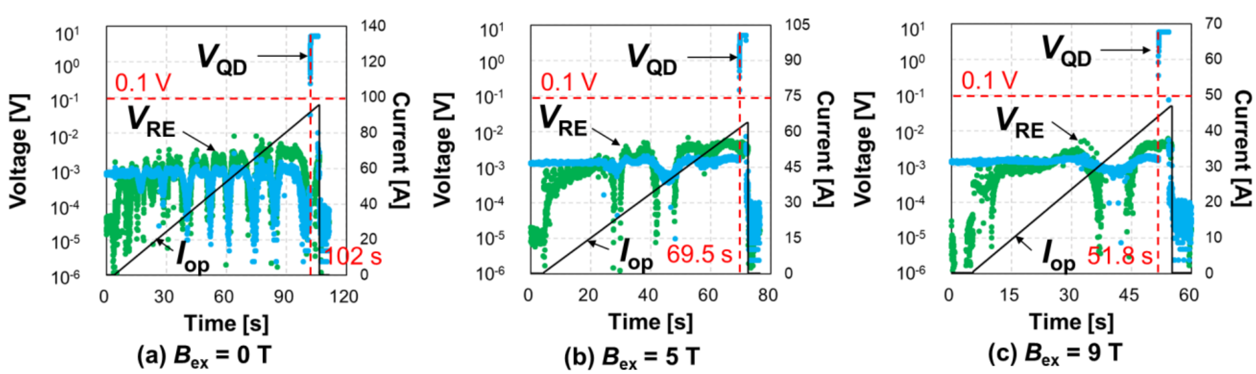

Fig. 8 Results of quench detection experiment with insulated REBCO coil at α_{op} = 1 A/s: (a) B_{ex} = 0 T, (b) B_{ex} = 5 T, and (c) B_{ex} = 9 T

thermal runaway in the REBCO coil where I_{op} is ~172 A, which is improved more than 10 times by the co-winding method compared to [39]. Since the current ramp rate is slow in the 30-T-class coil (< 1 A/s [51]–[53]), more time margin would be expected and it will be sufficient for the quench protection with a-few-seconds current damp. Thus, it was experimentally demonstrated that the implementation of the LTS QD would be effective for the quench protection system of the application under magnetic field.

B. Quench detection performance of Nb-Ti/Cu-Ni QD for NI/MI REBCO coils

The turn-to-turn resistivity was estimated for the NI and MI REBCO coils (ρ_t). Table VI lists ρ_t of the NI and MI coils which is multiples of the turn-to-turn resistance (R_t) and bonding area of the voltage taps (1 mm × 3 mm). By applying the current (I_t) and measuring the voltage in V_{tt} and V_{tb} as shown in Fig. 4, R_t was estimated by mean value of the proportional coefficient of I_t and V_{tt}, I_t and V_{tb}. Fig. 9 illustrates a simplified circuit of the NI/MI REBCO coils based on the partial element equivalent circuit (PEEC) model [54] where $R_{coil,\ r}$, $R_{coil,\ \theta}$, and L_{coil} are resistance in the radial direction, resistance in the circumferential direction, and inductance, respectively. Table VI also lists their calculated values. Mean value of inner and outer diameters was considered as coil diameter for the calculation. I_r and I_θ are the currents in the radial and circumferential directions, respectively. If I_θ is 0 A at initial condition, I_θ becomes

$$I_\theta = C_1\left\{\exp\left(-\frac{t}{\tau}\right) - 1\right\} + C_2\alpha_{op}t, \tag{3}$$

where

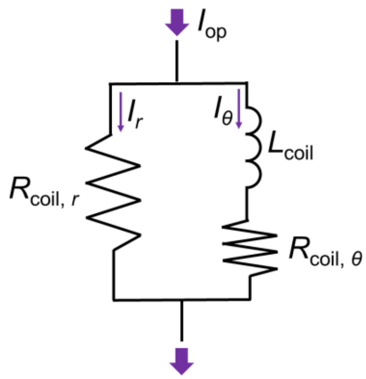

Fig. 9 Simplified circuit model of the NI and MI REBCO coils based on the PEEC model [54]

Table VI Local turn-to-turn resistivity (ρ_t), anisotropic resistances ($R_{coil,\ r}$ and $R_{coil,\ \theta}$), and inductance (L_{coil}) of the NI and MI REBCO coils

Coils	ρ_t	$R_{coil,\ r}$	$R_{coil,\ \theta}$	L_{coil}
NI	0.95 μΩcm²	59 μΩ	~ 0 at superconducting state except for the degraded region	13 μH
MI	2.1 μΩcm²	129 μΩ	~ 0 at superconducting state except for the degraded region	13 μH

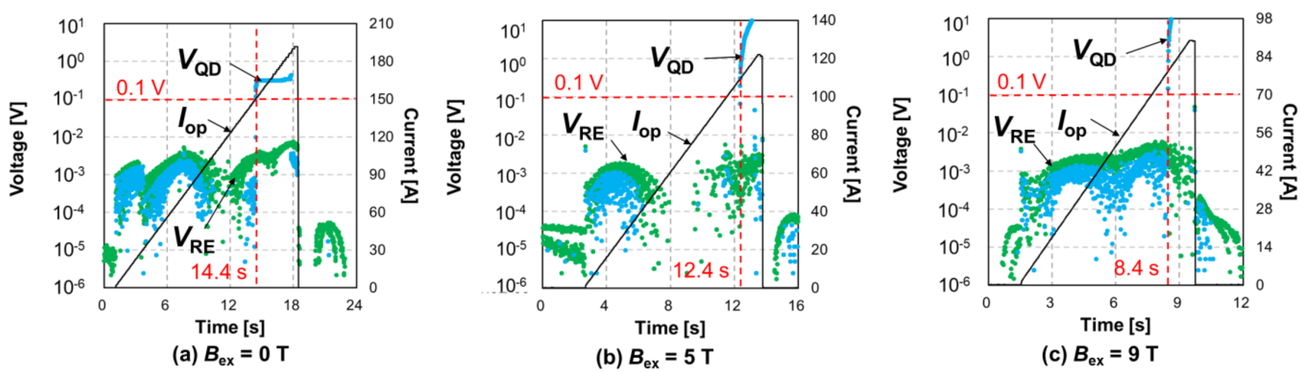

Fig. 10 Results of the quench detection experiment with MI REBCO coil at α_{op} = 10 A/s: (a) B_{ex} = 0 T, (b) B_{ex} = 5 T, and (c) B_{ex} = 9 T

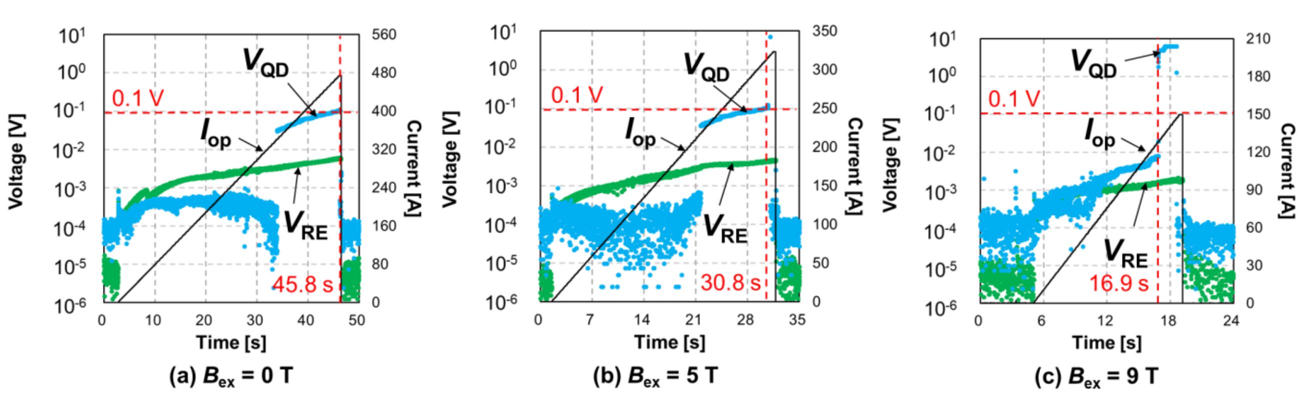

Fig. 11 Results of the quench detection experiment with NI REBCO coil at α_{op} = 10 A/s: (a) B_{ex} = 0 T, (b) B_{ex} = 5 T, and (c) B_{ex} = 9 T

Table VII Parameters on the equation (3) calculated by the equations (4)–(6) for the NI and MI REBCO coils

Coils	C_1	C_2	τ
NI	1.29 A	0.76	0.17 s
MI	0.78 A	0.87	0.089 s

$$C_1 = \frac{R_{\text{coil},\,r} L_{\text{coil}} \alpha_{\text{op}}}{\left(R_{\text{coil},\,r} + R_{\text{coil},\,\theta}\right)^2}, \tag{4}$$

$$C_2 = \frac{R_{\text{coil},\,r}}{R_{\text{coil},\,r} + R_{\text{coil},\,\theta}}, \tag{5}$$

$$\tau = \frac{L_{\text{coil}}}{R_{\text{coil},\,r} + R_{\text{coil},\,\theta}}. \tag{6}$$

Table VII lists the calculated C_1, C_2, and τ. Since L_{coil} is small in this experiment, first term on the right-hand side in the equation (3) become small (< 1.3 A) and I_θ becomes nearly $I_{\text{op}} = a_{\text{op}}t$. This indicates that the coil current mostly flows in the circumferential direction except in the degraded region. Thus, the quench of LTS QD would be induced only by the local heating around the hot-spot in the REBCO coil. In the case of the NI/MI REBCO coils with large inductance, the heating due to I_r would increase the temperature of the LTS QD. This shall be considered in the design of the LTS QD.

Table V lists the t_{QD} and I_{opQD} in the NI and MI REBCO coils for different B_{ex}. Fig. 10 shows the voltage in the Nb–Ti/Cu–Ni QD (V_{QD}) and MI REBCO coil (V_{RE}), and coil operation current (I_{op}) at B_{ex} = 0, 5, and 9 T. I_{opQD} (t_{QD}) was 147 A (14.4 s), 109 A (12.4 s), and 79.7 A (8.4 s) at B_{ex} = 0 T, 5 T, and 9 T, respectively. I_{opQD} is 2.8–5.1 times larger than that of the insulated coil shown in Fig. 6 and Table V. The heat density around the hot spot may influence the behavior of V_{QD} in terms of the initiation of the normal zone in the LTS QD. Heat can easily diffuse around the hot spot in the MI coil compared to the case of an insulated coil with an insulating material having low thermal conductivity. Further, turn-to-turn current sharing reduces the heat density around the hot spot. These led to a slow temperature rise in the Nb–Ti/Cu–Ni QD and larger I_{opQD} than in the case of the insulated REBCO coil. The change in V_{QD} with respect to time was more gradual than that shown in Fig. 6. Fig. 11 shows V_{RE}, V_{QD}, and I_{op} for the NI coil at B_{ex} = 0 T, 5 T, and 9 T. I_{opQD} (t_{QD}) was 472 A (45.8 s), 313 A (30.8 s), and 133 A (16.9 s) at B_{ex} = 0 T, 5 T, and 9 T, respectively. This result shows slower quench detection than in the case of the MI coil. This also might be caused by the difference in the heat density around hot spot of the REBCO coil. The turn-to-turn resistance of the coil would be one of the key parameters. The ρ_t of the MI coil was higher than that of the NI coil as shown in Table VI. Thus, it is considered the larger heat density around the hot spot contributed the quicker initiation of the normal zone in the LTS QD in the case of the MI coil.

C. Normal zone propagation in LTS QD co-wound in insulated, NI, and MI REBCO coils

Table VIII NZPV_{exp} estimated from the equation (9) and h_{eff} giving agreement between NZPV_{eq} and NZPV_{exp}

Coils	B_{ex}	NZPV_{exp}	h_{eff}
Insulated	0 T	5.12×10^{-1} m/s	2.39×10^3 W/m^{2}K
	5 T	6.30×10^{-1} m/s	2.27×10^3 W/m^{2}K
	9 T	1.79 m/s	2.15×10^3 W/m^{2}K
MI	0 T	2.35×10^{-1} m/s	2.84×10^3 W/m^{2}K
	5 T	4.77×10^{-1} m/s	2.55×10^3 W/m^{2}K
	9 T	1.52 m/s	2.67×10^3 W/m^{2}K
NI	0 T	2.32×10^{-4} m/s	3.18×10^3 W/m^{2}K
	5 T	2.96×10^{-4} m/s	3.31×10^3 W/m^{2}K
	9 T	1.10 m/s	3.40×10^3 W/m^{2}K

Table IX The constants used for the calculation of NZPV_{eq} and NZPV_{exp} defined in the equations (7) and (8)

Constants	Values
I_{m}	0.31 A
P	0.24 mm
A	4.4×10^{-3} mm^2
ρ_{QD}	0.36 μΩm at 0 T 0.36 μΩm at 5 T 0.36 μΩm at 9 T
C_{QD}	20.1. kJ/m^{3}K at 0 T 20.1. kJ/m^{3}K at 5 T 12.1 kJ/m^{3}K at 9 T
κ_{QD}	3.14 W/mK at 0 T 3.03 W/mK at 5 T 2.14 W/mK at 9 T
T_{cs}	9.4 K at 0 T 9.2 K at 5 T 7.4 K at 9 T

After the initiation of the normal zone in the LTS QD, normal zone propagation velocity (NZPV) determines V_{QD}. Thermal diffusion from the LTS QD to the REBCO coil may highly influence the NZPV in the LTS QD. V_{QD} quickly reaches 0.1 V in the cases of the insulated (Fig. 6) and MI coils (Fig. 10), while V_{QD} reaches 0.1 V with gradual increase in the case of the NI coil at B_{ex} = 0 T and 5 T (Fig. 11). This different behavior indicates the difference in NZPV. A simplified NZPV for the LTS QD (NZPV_{eq}) can be expressed by the following equation [55],

$$\text{NZPV}_{\text{eq}} = \frac{\Gamma - 2}{C_{\text{QD}}(\Gamma - 1)} \sqrt{\frac{P \kappa_{\text{QD}} h_{\text{eff}}}{A}}, \tag{7}$$

$$\Gamma = \frac{I_{\text{m}}^2 \rho_{\text{QD}}}{A P h_{\text{eff}} \theta_{\text{cs}}}, \tag{8}$$

where A, P, ρ_{QD}, C_{QD}, and κ_{QD} are cross-sectional area, perimeter, equivalent resistivity, equivalent heat capacity, and equivalent thermal conductivity of the LTS QD at its T_{cs}. The heat transfer coefficient of the coolant is normally used as h_{eff}, while h_{eff} corresponds to the thermal conductance between the REBCO coil and the LTS QD in this study. Although too small h_{eff} may delay the initiation of normal zone in the LTS QD, smaller h_{eff} would lead to larger NZPV resulting in the quicker voltage increase in the LTS QD. θ_{cs} is defined as the difference between T_{cs} of the LTS QD and temperature of the REBCO coil. According to the experimental results, V_{RE} is almost proportional to the I_{op} indicating the normal zone propagation in the REBCO coil is negligible. Then, it can be assumed that the boundary of normal zone in the LTS QD always faces to the REBCO tape at superconductive state at ~ T_{op} = 4.2 K. Thus, θ_{cs} can be approximated as $\theta_{cs} \sim T_{cs} - 4.2$ K. Table VIII lists the NZPV calculated from the time derivative of V_{QD} around V_{QD} = 0.1 V by the following equation (NZPV$_{exp}$).

$$\mathrm{NZPV_{exp}} = \frac{A}{\rho_{QD}} \frac{\mathrm{d}V_{QD}}{\mathrm{d}t}\bigg|_{V_{QD}(t)\sim 0.1\ \mathrm{V}} . \quad (9)$$

Table IX lists the value of the constants used for the calculation of NZPV$_{eq}$ and NZPV$_{exp}$. Electrical resistivity, heat capacity, and thermal conductivity of Nb-Ti and Cu-Ni were referred from [56]–[58]. NZPV$_{exp}$ became smaller than the general NZPV of the LTS wire, such as 1–100 m/s, because of the small load factor of the I_m. When h_{eff} remains constant, the equations (7) and (8) indicate that NZPV$_{exp}$ does not change if the specification of the LTS QD and B_{ex} are the same. However, the different coils show different NZPV$_{exp}$ even with the same LTS QD at the same B_{ex}. Table VIII also lists the h_{eff} which gives agreement between the NZPV$_{exp}$ and NZPV$_{eq}$. h_{eff} shows different value in the different REBCO coil, while it does not show obvious dependence on B_{ex} in the same REBCO coil. Thus, it can be regarded as a parameter featuring the thermal diffusion from the LTS QD to a certain REBCO coil. The largest and smallest thermal diffusion are indicated in the cases of the NI REBCO coil with largest h_{eff} and insulated REBCO coil with smallest h_{eff}, respectively. Although there might be contribution of thermal contact resistance between the LTS QD and REBCO coil, the result is quantitatively reasonable by considering the thermal diffusivity of materials around the LTS QD. For instance, thermal diffusivities of polyimide, austenitic stainless steel, and copper (RRR = 30) are, 9.8×10^{-6} m^2/s, 1.2×10^{-5} m^2/s, and 0.2 m^2/s, respectively [57], [59], [60]. This result shows thermal conductance between the LTS QD and REBCO coil would be a key parameter to design the LTS QD in terms of both initiation of normal zone and normal zone propagation in the LTS QD.

The results indicated the key parameters for the behavior of the LTS QDs in the REBCO coils, and the feasibility of the quench detection with the LTS QD for three types of REBCO pancake coils (insulated, NI, MI) was demonstrated at 4.2 K and 0–9 T. For future research, further experimental demonstrations with LTS QDs for higher magnetic field applications or higher operation temperatures (such as Nb_3Al, iron-based super-conductors, and MgB_2) are required. Recent studies [61]–[63] indicate that the flexible Nb_3Al wires with a dimeter of 30–80 μm show small difference between critical current density with the wind-and-react and react-and-wind processes. Thus, it would be a good option to use the thin Nb_3Al wire as LTS QD without reducing the engineering current density of the REBCO coil. Similarly, LTS QDs with a higher critical temperature (T_c), such as, MgB_2 and iron-based superconducting QDs are expected to be used even at > 4.2 K as suggested in [43], [45], [46]. Falese quench detection by the low-T_c LTS QD due to its small temperature margin would be concerned in the real case. The higher-T_c LTS QDs would mitigate this risk although this should be discussed with their sensitivity in further studies.

IV. Conclusion

In this study, the quench detection performance of LTS QDs for insulated, NI, and MI REBCO coils cooled with LHe was investigated. This study indicated the key parameters related to the behavior of the LTS QDs in the REBCO coils, and demonstrated the feasibility of the quench detection with appropriate LTS QDs for three types of REBCO pancake coils (insulated, NI, MI) operated at 4.2 K and 0–9 T.

Experiments demonstrated the quench detection before thermal runaway in insulated, NI, and MI REBCO pancake coils with Nb–Ti/Cu–Ni QDs at 4.2 K and 0–9 T. Compared the results in the cases of insulated, NI, and MI REBCO coils, it was also quantitatively demonstrated that the turn-to-turn resistance and thermal gap conductance were key parameters to design the LTS QD in terms of the initiation of quench and normal zone propagation in the LTS QD.

Acknowledgement

This work was performed at the High Field Laboratory for Supercon-ducting Materials (HFLSM), Institute for Materials Research, Tohoku University (Project No. 20H0205). We would like to thank Editage (www.editage.com) for English language editing.

References

[1] F. Trillaud *et al.*, "Normal Zone Propagation Experiments on HTS Composite Conductors", *Cryogenics*, Vol. 43, pp. 271–279, 2003

[2] X. Wang *et al.*, "Normal Zone Initiation and Propagation in Y-Ba-Cu-O Coated Conductors with Cu Stabilizer", *IEEE Trans. Appl. Supercond.*, Vol. 15, pp. 2586–89, 2005

[3] H. H. Song and J. Schwartz, "Stability and Quench Behavior of $YBa_2Cu_3O_{7-x}$ Coated Conductor at 4.2K, Self-field", *IEEE Trans. Appl. Supercond.*, Vol. 19, pp. 3735–3743, 2009

[4] X. Wang, U. P. Trociewitz, and J. Schwartz, "Self-field Quench Behavior of $YBa_2Cu_3O_{7-\delta}$ Coated Conductors with Different Stabilizers", *Supercond. Sci. Technol.*, Vol. 22, 085005, 2009

[5] O. Tsukamoto, Y. Fujimoto and T. Takao, "Study on Stabilization and Quench Protection of Coils Wound of HTS Coated Conductors Considering Quench Origins – Proposal of Criteria for Stabilization and Quench Protection", *Cryogenics*, Vol. 63, pp. 148–154, 2014

[6] R. Heller *et al.*, "Conceptual Design Improvement of a Toroidal Field Coil for EU DEMO Using High-Temperature Superconductors", *IEEE Trans. Appl. Supercond.*, Vol. 26, 4201105, 2016

[7] S. Nie *et al.*, "Quench Detection for HTS SMES", *IEEE Trans. Appl. Supercond.*, Vol. 25, 5700605, 2015

[8] T. Ariyama *et al.*, "Quench Protection of YBCO Coils: Co-Winding Detection Method and Limits to Hot-Spot Temperature", *IEEE Trans. Appl. Supercond.*, Vol. 26, 4702205, 2016

[9] T. Ariyama *et al.*, "Quench protection system for an HTS coil that uses Cu tape co-wound with an HTS tape", *Supercond. Sci. Technol.*, Vol. 32, 115016, 2019

[10] T. Wang *et al*., “Detection method for a local normal-state transition in a No-Insulation REBCO pancake coil”, *IEEE Trans. Appl. Supercond.*, Vol. 27, 0601206, 2017

[11] A. Kawagoe *et al*., “Non-contact detection of normal transitions in superconducting coils—Application to monitoring systems for windings in HTS superconducting transformers during operation—", *TEION KOGAKU (J. Cryo. Super. Soc. Jpn.)*, Vol. 47, pp. 268–275, 2012

[12] H. Hiwatashi *et al*., “Detection of Local Abnormalities in Windings of High-Temperature Superconducting Transformers by Using Pick-Up Coils”, *IEEE Trans. Appl. Supercond.*, Vol. 24, 9001104, 2014

[13] H. Lee *et al*., “Detection of ‘Hot Spots’ in HTS Coils and Test Samples With Acoustic Emission Signals”, *IEEE Trans. Appl. Supercond.*, Vol. 14, pp. 1298–1301, 2004

[14] M. Marchevsky *et al*., “Acoustic thermometry for detecting quenches in superconducting coils and conductor stacks”, *Appl. Phys. Lett.*, Vol. 110, 12601, 2017

[15] M. Marchevsky *et al*., “Quench Detection for High-Temperature Superconductor Conductors Using Acoustic Thermometry”, *IEEE Trans. Appl. Supercond.*, Vol. 28, 4703105, 2018

[16] F. Trillaud *et al*., “Protection and quench detection of YBCO coils results with small test coil assemblies”, *IEEE Trans. Appl. Supercond.*, Vol. 17, pp. 2450–2453, 2007

[17] M. Yoneda *et al*., “Quench detection/protection of an HTS coil by AE signals”, *Physica C*, Vol. 471, pp. 1432–1435, 2011

[18] F. Scurti *et al*., “Quench detection for high temperature superconductor magnets: a novel technique based on Rayleigh-backscattering interrogated optical fibers”, *Supercond. Sci. Technol.*, Vol. 29, 03LT01, 2016

[19] F. Scurti *et al*., “Optical fiber distributed sensing for high temperature superconductor magnets”, *Supercond. Sci. Technol.*, Vol. 30, 114002, 2017

[20] Y. Liu *et al*., “Feasibility Study of Fiber Bragg Grating Sensor for Quench Detection of High Temperature Superconductors”, *IEEE Trans. Appl. Supercond.*, Vol. 29, 9001606, 2019

[21] C. D. Van der Laan *et al*., “CORC® wires containing integrated optical fibers for temperature and strain monitoring and voltage wires for reliable quench detection”, *Supercond. Sci. Technol.*, Vol. 33, 085010, 2020

[22] B. Chen *et al*., “Distributed optical fiber sensor for investigation of normal zone propagation and hot spot location in REBCO cables”, *Fusion Eng. Des.*, Vol. 156, 111569, 2020

[23] Y. Liu *et al*., “Application of Epoxy-Bonded FBG Temperature Sensors for High-Temperature Superconductor-Coated Conductor Quench Detection”, *IEEE Trans. Appl. Supercond.*, Vol. 31**,** 4700308, 2021

[24] J. Jiang *et al*., “Experimental study on quench detection of a no-insulation HTS coil based on Raman-scattering technology in optical fiber”, *IEEE Trans. Appl. Supercond.*, Vol. 28, 4702105, 2018

[25] J. Jiang *et al*., “Spatial and Temporal Resolution Optimization on Raman Distributed Temperature Sensor System for Quench Detection in a No-Insulated Coil”, *IEEE Trans. Appl. Supercond.*, Vol. 29, 9001105, 2019

[26] J. Jiang *et al*., “Thermal Stability Study of a Solder-Impregnated No-Insulation HTS Coil Via a Raman-Based Distributed Optical Fiber Sensor System”, *IEEE Trans. Appl. Supercond.*, Vol. 29, 9000604, 2019

[27] E. Ravaioli *et al*., “A new quench detection method for HTS magnets: stray-capacitance change monitoring”, *Phys. Scr.*, Vol. 95, 015002, 2020

[28] S. Hahn, D. K. Park, J. Bascunan, and Y. Iwasa, “HTS Pancake Coils Without Turn-to-Turn Insulation”, *IEEE Trans. Appl. Supercond.*, Vol. 21, pp. 1592–1595, 2011

[29] K. R. Bhattarai *et al*., “Understanding Quench in No-insulation (NI) REBCO Magnets through Experiments and Simulations”, *Supercond. Sci. Technol.*, Vol. 33, 035002, 2020

[30] H. Song and Y. Wang, “Simulations of Nonuniform Behaviors of Multiple No-Insulation (RE)$Ba_2Cu_3O_{7-x}$ HTS Pancake Coils During Charging and Discharging”, *IEEE Trans. Appl. Supercond.*, Vol. 26, 4700105, 2016

[31] S. An *et al*., “A Feasibility Study on ‘Magnetic Dam’ to Absorb Magnetic Energy in NI HTS Magnet During Quench”, *IEEE Trans. Appl. Supercond.*, Vol. 30, 4701705, 2020

[32] X. Wang *et al*., “Turn-to-turn Contact Characteristics for an Equivalent Circuit Model of No-insulation ReBCO Pancake Coil”, *Supercond. Sci. Technol.*, Vol. 26, 035012, 2013

[33] S. Noguchi *et al*., “Turn-to-Turn Contact Resistance Measurement of No-Insulation REBCO Pancake Coils”, *IEEE Trans. Appl. Supercond.*, Vol. 29, 4601605, 2019

[34] K. Kim *et al*., “Quench Behavior of a No-insulation Coil Wound with Stainless Steel Cladding REBCO Tape at 4.2 K”, *Supercond. Sci. Technol.*, Vol. 30, 075001, 2017

[35] J. Kim *et al*., “Effect of resistive metal cladding of HTS tape on the characteristic of no-insulation coil”, *IEEE Trans. Appl. Supercond.*, Vol. 26, 4601906, 2016

[36] T. Lécrevisse *et al*., “Metal-as-insulation Variant of No-insulation HTS Winding Technique: Pancake Tests under High Background Magnetic Field and High Current at 4.2 K”, *Supercond. Sci. Technol.*“, Vol. 31, 055008, 2018

[37] F. Dong *et al.*, “On fault-mode phenomenon in no-insulation superconducting magnets: A preventive approach”, *Appl.Phys.Lett.*, Vol. 121, 194101, 2022

[38] S. Hasegawa *et al*., “Numerical and Experimental Evaluations of the Quench Detection Performance of a REBCO/Nb–Ti_d Tape”, *IEEE. Trans. Appl. Supercond.*, Vol. 28, 4700605, 2018

[39] S. Hasegawa *et al*., “Fundamental Evaluations of Applicability of LTS Quench Detectors to REBCO Pancake Coil”, *IEEE. Trans. Appl. Supercond.*, Vol. 29, 9001305, 2019

[40] S. Hasegawa *et al.*, “Quench Detection Performance of Low-temperature Superconducting Quench Detectors for REBCO Tape in Magnetic Fields”, *IEEE. Trans. Appl. Supercond.*, Vol. 31, 4701605, 2021

[41] A. V. Dudarev, *et al*., “Quench Propagation and Detection in the Superconducting Bus-bars of the ATLAS Magnets”, *IEEE. Trans. Appl. Supercond.*, Vol. 10, pp. 381–384, 2000

[42] A. Dudarev *et al*., “New Fast Response Thin Film-Based Superconducting Quench Detectors”, *IEEE. Trans. Appl. Supercond.*, Vol. 24, 8800204, 2014

[43] R. Kang, J. Wang and Q. Xu, “Detecting Quench in HTS Magnets With LTS Wires—A Theoretical and Numerical Analysis”, *IEEE Trans. Appl. Supercond.*, Vol. 32, 4701905, 2022

[44] R. Kang *et al.*, “Toward an Encapsulated LTS Quench Detector for Fast Quench Detection in HTS Magnets”, *IEEE Trans. Appl. Supercond.*, Vol. 34, 4604705, 2024

[45] N. Bykovskiy, *et al.*, "Co-Wound Superconducting Wire for Quench Detection in Fusion Magnets", *IEEE Trans. Appl. Supercond.*, Vol. 32, 2500105, 2022

[46] N. Bykovskiy, *et al.*, “Experiemtal study of stability, quench propagation and detection methods on 15 kA sub-scale HTS fusion conductors in SULTAN”, *Supercond. Sci. Technol.*, Vol. 36, 034002, 2023

[47] T. S. Lee, *et al*., “The effects of co-wound Kapton, stainless steel and copper, in comparison with no insulation, on the time constant and stability of GdBCO pancake coils”, *Supercond. Sci. Technol.*, Vol. 27, 065018, 2014

[48] Y. Suetomi, *et al.*, “Quench and self-protecting behaviour of an intra-layer no-insulation (LNI) REBCO coil at 31.4 T”, *Supercond. Sci. Technol*, Vol. 34, 064003, 2021

[49] Superpower Inc., “2G HTS Wire Specification”, https://www.superpower-inc.com/specification.aspx, 2024

[50] K. Tsuchiya, et al., “Critical current measurement of commercial REBCO conductors at 4.2 K”, *Cryogenics*, Vol. 85, pp. 1–7, 2017

[51] H. Maeda *et al*., “Development of Super-high-field NMR Operated Beyond 1 GHz Using High Temperature Superconducting coil”, *eMagRes*, Vol. 5, pp. 1109–1120, 2016

[52] H. W. Weijers *et al*., “Progress in the Development and Construction of a 32-T Superconducting Magnet”, *IEEE Trans. Appl. Supercond*., Vol. 26, 4300807, 2016

[53] H. Maeda *et al*., “The MIRAI Program and the New Super-High Field NMR Initiative and Its Relevance to the Development of Superconducting Joints in Japan”, *IEEE Trans. Appl. Supercond*., Vol. 29, 4602409, 2019

[54] T. Wang *et al.*, “Analyses of Transient Behaviors of No-Insulation REBCO Pancake Coils During Sudden Discharging and Overcurrent”, *IEEE Trans. Appl. Supercond.*, Vol. 25, 4603409, 2015

[55] M. N. Wilson, “Superconducting Magnets”, Clarendon Press, 1987

[56] P Bauer *et al.*, “EFDA material data compilation for superconductor simulation”, EFDA CSU, Garching, April, 2007

[57] J. H. Hucek *et al.*, “Handbook on Materials for Superconducting Machinery Includes Data Sheets for First and Second Supplements Colorado: National Bureau of Standards Cryogenics Division-Boulder”, 1975

[58] H. Brechna, “Superconducting Magnet Systems”, Springer, 1973

[59] D. L. Rule *et al.*, “Thermal Conductivity of a Polyimide Film between 4.2 and 300 K, with and without Alumina Particles as Filler”, NISTIR 3948, August 1990

[60] D. Mann, “LNG materials and fluids: a user's manual of property data in graphic format”, NIST, January 1977

[61] A. Kikuchi *et al.*, "Ultra-Fine Nb3Al Mono-Core Wires and Cables,", *IEEE Trans. Appl. Supercond.*, Vol. 31, 6000105, 2021

[62] A. Kikuchi *et al.*, "The Bronze Processed Nb3Sn Ultra-Thin Superconducting Wires", *IEEE Trans. Appl. Supercond.*, Vol. 32, 6000104, 2022

[63] A. Kikuchi, *et al*,. “Mechanical Properties of Ultra-Thin Nb_3Sn Composite Wires”, *IEEE Trans. Appl. Supercond*,.Vol. 33. 8400905, 2023